PNAS nexus

PNAS Nexus, 2022, **1**, 1–9
https://doi.org/10.1093/pnasnexus/pgac028
Advance access publication date: 16 March 2022
Research Report

Sensitive, smartphone-based SARS-CoV-2 detection from clinical saline gargle samples

Lane E. Breshears[a,1], Brandon T. Nguyen[a,1], Patarajarin Akarapipad[a,1], Katelyn Sosnowski[a,1], Kattika Kaarj[b], Grace Quirk[c], Jennifer L. Uhrlaub[d], Janko Nikolich-Žugich[d], Michael Worobey[c] and Jeong-Yeol Yoon[a,*]

[a]Department of Biomedical Engineering, The University of Arizona, Tucson, AZ 85721, USA
[b]Department of Biosystems Engineering, The University of Arizona,Tucson, AZ 85721, USA
[c]Department of Ecology and Evolutionary Biology, The University of Arizona, Tucson, AZ 85721, USA
[d]Department of Immunobiology, The University of Arizona College of Medicine,Tucson, AZ 85724, USA
*To whom correspondence should be addressed: Email: jyyoon@arizona.edu
Edited By: Bruce Levine

Abstract

Saliva specimens have drawn interest for diagnosing respiratory viral infections due to their ease of collection and decreased risk to healthcare providers. However, rapid and sensitive immunoassays have not yet been satisfactorily demonstrated for such specimens due to their viscosity and low viral loads. Using paper microfluidic chips and a smartphone-based fluorescence microscope, we developed a highly sensitive, low-cost immunofluorescence particulometric SARS-CoV-2 assay from clinical saline gargle samples. We demonstrated the limit of detection of 10 ag/μL. With easy-to-collect saline gargle samples, our clinical sensitivity, specificity, and accuracy were 100%, 86%, and 93%, respectively, for $n = 27$ human subjects with $n = 13$ RT-qPCR positives.

Keywords: clinical samples, microfluidics, biosensor, smartphone, COVID-19, immunoassay, point-of-care, smartphone-based fluorescence microscope

Significance Statement:

A novel diagnostic method based on a smartphone fluorescence microscope and paper microfluidic chip is introduced for SARS-CoV-2 detection. It utilizes self-collectable saline gargle sampling, preventing unnecessary virus exposure to healthcare providers. No dilution, purification, filtration, or extraction are required. An extremely low limit of detection, down to 10 ag/μL (subsingle copy), is demonstrated. Clinical sensitivity of 100% and clinical accuracy of 93% are demonstrated for $n = 27$ clinical samples with $n = 13$ RT-qPCR positives. The method can easily be adapted to other respiratory viruses by changing antibodies and optimizing the assay for target concentrations.

Introduction

Diagnosis of viral respiratory infections, including the coronavirus disease 2019 (COVID-19), has typically been conducted by collecting nasopharyngeal or nasal swabs (1) and subsequently conducting either a rapid antigen assay (2–4) or RT-qPCR (2, 5). Both nasopharyngeal and nasal swabs may be uncomfortable to patients, and procedures in which the samples are not self-collected may increase the risk of infection for staff or caregivers. Very recently, saliva specimens have drawn interest as a potential sample collection method due to their ease of collection, speed, low cost, and decreased risk to healthcare providers (5, 6). However, samples may require dilution or pretreatment due to their viscosity, and antigens may be more challenging to detect in this specimen type (5). Depending on whether or not a patient's mouth contains food, beverage, tobacco, mouthwash, toothpaste, and so on before sample collection, significant contaminants may hinder the assay performance. At the University of Arizona, we have successfully developed and implemented a saline gargle sample collection method for use with the RT-qPCR COVID-19 assays (7). Individuals were given 5 mL of 0.9% w/v sterile NaCl (typical concentration of over-the-counter saline) and completed a 5-second swish followed by a 10-second gargle, all repeated 3 times, before collecting samples. Positive samples were confirmed by RT-qPCR using CDC RUO primers. The obvious next course of action is implementing this saline gargle collection method with a more rapid and portable immunoassay, as RT-qPCR requires complex laboratory equipment, is expensive to conduct, and may not be able to provide rapid (< 20 min) results in large populations (2, 3). However, the accuracy of rapid antigen assays has been questioned, especially for early-phase infections, asymptomatic infections, breakthrough infections, and viral variants (2, 3, 8, 9). This problem would be more pronounced with saliva samples, where the viral load would be substantially lower than in nasopharyngeal and nasal swab samples (6). We have previously demonstrated the

Competing Interest: The authors declare no competing interests.
[1]These authors contributed equally.
Received: November 20, 2021. **Revised:** January 21, 2022. **Accepted:** March 9, 2022

use of a smartphone-based fluorescence microscope and paper microfluidic particle immunoagglutination assay for single-copy detection of norovirus from spiked environmental water samples (10). Using EDAC binding protocols, 500-nm fluorescent particles were covalently conjugated to antibodies specific to the target antigen. Samples containing varying quantities of target antigen were loaded onto wax-based paper microfluidic chips. After drying, the prepared reagent with antibody-conjugated fluorescent particles was loaded onto the chip. Positive samples with antigen present consequentially underwent immunoagglutination, showing a clumping of fluorescent particles around target antigens. Negative samples had lower signals than positive samples. Using a method that we refer to as particulometry, we directly imaged and counted the total area of immunoagglutinated particles on the microfluidic channels using a smartphone-based fluorescence microscope, achieving high accuracy and low limit of detection (LOD). In this new work, we redesigned the device and method to accommodate human saline gargle samples toward accurate and low LOD detection of SARS-CoV-2 without dilution, purification, or pretreatment. Our specific aims were: (1) to design and optimize the smartphone assay device to detect SARS-CoV-2 from saline gargle samples, (2) to demonstrate extremely low LOD, preferably at the single virus copy level or better, (3) to detect the virus from clinical samples (rather than spiked water samples) without dilution, purification, or pretreatment, and (4) to demonstrate satisfactory clinical specificity, clinical sensitivity, and clinical accuracy, despite the different sample medium in saline gargle samples compared to that of nasopharyngeal and nasal swabs. Figure 1 is a visual schematic of the complete pipeline, including clinical saline gargle sample collection by the University of Arizona (top) and loading of samples and fluorescent-particle conjugated antibodies onto paper microfluidic chips (bottom). (The antibody–antigen reaction shown in Figure 1 illustrates the immunoagglutination reaction. However, as the number of potential binding sites for both the antibody and the antigen are high and variable, we cannot determine the exact avidity.) Our demonstrated method is a promising alternative to available testing methods due to its low cost, relatively high sensitivity, and ability to work with both high and low concentrations of antigen in an accessible sample medium (saline gargle samples). This tool could also be highly useful for future pandemics, variant detection, and/or antibody detection, as it is capable of being adapted for novel targets.

Materials and Methods

Preparation of antibody-conjugated fluorescent particles

Targeted detection of the SARS-CoV-2 viral antigens was performed by tracking the extent of particle immunoagglutination. Rabbit polyclonal antibodies to SARS-CoV-2 nucleocapsid protein (40143-T62 100 μL; Sino Biological; Beijing, China) were conjugated to 0.5 μm diameter, yellow–green fluorescent, carboxylated polystyrene particles (CAF-005UM; Magsphere, Inc., Pasadena, CA). The specific version used in this paper can be found on protocols.io at https://doi.org/10.17504/protocols.io.bhsvj6e6. The process used 1 mg/mL 1-ethyl-3-(3-dimethylaminopropyl)carbodiimide (EDAC; E7750; Sigma–Aldrich, St. Louis, MO) as a crosslinker to covalently couple the amine groups of anti-SARS-CoV-2 IgG antibodies to carboxyl groups on the particles, forming peptide bonds. Bovine serum albumin (BSA; BP700100; Thermo Fisher Scientific, Waltham, MA) was used as a blocking agent to prevent nonspecific hydrophobic interactions between particles. After conjugation of particles, the final particle concentration was estimated using a miniature spectrophotometer (USB4000; Ocean Optics, Dunedin, FL) at 488 nm (excitation wavelength of the fluorescent particles) and compared to a previously constructed standard curve. Undiluted, stock antibody-conjugated particles could be kept in the refrigerator at 2–8°C for up to 2 weeks. We found that sonicating the stock antibody-conjugated particle solutions for 10 min daily helped prevent self-aggregation. Antibody-conjugated fluorescent particles were diluted to 40 ng/μL in a solution containing 0.05% (v/v) Tween 20 and storage buffer (1 mg BSA dissolved in 10 mL DI water) at a 1:3 (Tween 20:particles + storage buffer) ratio. After adding Tween 20, the particle suspension was used within the next 24 h. Before performing experiments, the diluted suspension was sonicated for 10 min and then 1 μL of the final solution was imaged under the benchtop fluorescence microscope to check for self-aggregation. Typically, the particles would require an additional soft-wash step to eliminate any large aggregates. A total of 1–2 rounds of centrifugation at 8,200 g for 2 min (saving only the supernatant) was performed until self-aggregation was minimized.

Preparation of wax-printed paper-based microfluidic chips

Wax-printed paper-based microfluidic chips were prepared according to the protocol described in Chung et al. (10). Briefly, chips were printed onto nitrocellulose paper (UniSart CN 95 with polyester backing, 100 μm thickness; Sartorius Stedim Biotech, Goettingen, Germany) using a wax printer (Xerox ColorQube 8580, Norwalk, CT). Next, chips were placed face-up on a hot plate (MS-H-Pro+; SciLogex, Rocky Hill, CT) and heated underneath a metal weight covered in aluminum foil for 3 min at 120°C. The backs of the chips were inspected to make sure the wax had consistently melted through the depth of the paper, and chips were heated for a longer time if needed to ensure consistent wax melting. Any chips with visible debris inside the borders of the channels were discarded. Chips were cooled for at least 5 min before storing in a container. Protocol for wax printing the paper microfluidic chips is available on protocols.io at https://dx.doi.org/10.17504/protocols.io.btqxnmxn.

Design and assembly of smartphone-based fluorescence microscope device

We developed a low-cost and handheld smartphone-based fluorescence microscope device to collect optical signal from yellow–green fluorescent particles. Since the particles have an excitation wavelength of 488 nm and emission wavelength of 509 nm, a 460-nm LED (WP7113QBC/G; Digi-Key, Thief River Falls, MN) covered with a band-pass color filter film (Roscolux Color Filter Booklet; Edmund Optics, Barrington, NJ) was used as the excitation light source. This LED provided enough intensity at the target excitation wavelength while avoiding overlap with the emission signal of the particles. An additional white LED (HM-13052; Chanzon, Shenzhen, China) was incorporated into the circuit to illuminate the chip while the user located the channels, and a switch allowed the user to toggle between the white light (for chip alignment) and the blue light (for fluorescence imaging). A color filter film with a cut-on wavelength of 500 nm (Roscolux Color Filter Booklet; Edmund Optics) was used as a low-cost emission filter by placing it between the microscope and smartphone camera. The device housing was designed in SolidWorks R2020 (Dassault Systèmes, Vélizy-Villacoublay, France) to enclose a 100X–250X pocket microscope (B07NW5Z3WF; Carson Optical, Ronkonkoma,

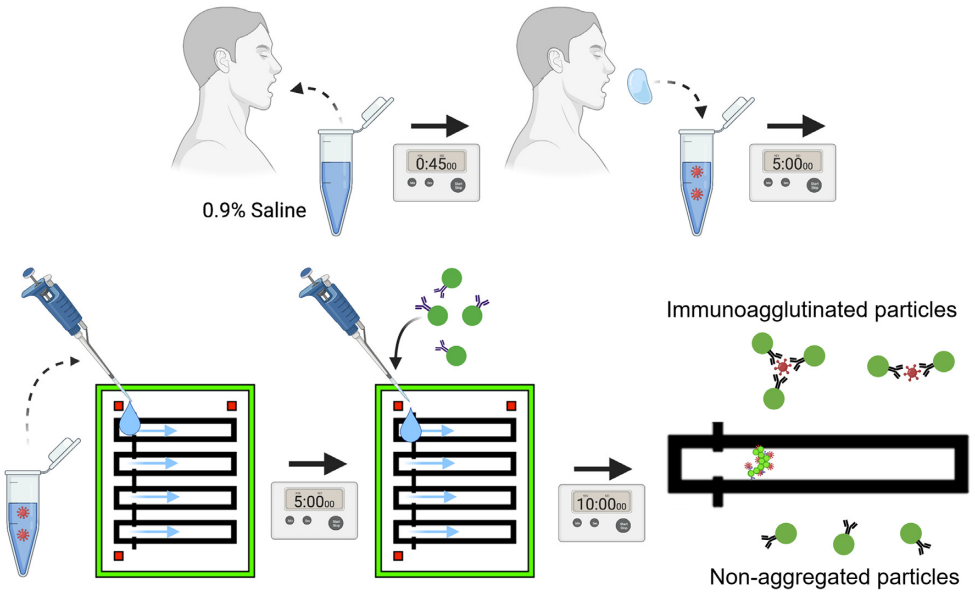

Fig. 1. Outline of the assay process. Saline gargle samples were collected and loaded onto paper-based microfluidic chips. Antibody-conjugated fluorescent particles were then loaded, and the flow through the paper microfluidic channels occurred passively through capillary action. This mixing led to particle immunoagglutination, which was quantified with a smartphone-based fluorescence microscope. This figure was created using BioRender.com.

NY), which represents the main optical module, providing a dark environment for fluorescence imaging. The excitation light source, powered by a rechargeable 9 V battery, was installed inside the housing. A smartphone camera (Galaxy S20; Samsung Electronics America, CA) was used to image the fluorescence signal. The foldable smartphone stand designed in SolidWorks can extend from the top to rest the smartphone steadily while taking images and fold flat for carrying when the device is not in use. All parts designed in SolidWorks were 3D printed using Creality Ender-3 (Creality 3D, Shenzhen, China) with PETG filament (Overture 3D, Wilmington, DE). Design details are described in Supplementary Figures S1–S9 (Supplementary Material).

Saline gargle samples

SARS-CoV-2 Isolate USA-WA1/2020 samples obtained from the US Centers for Disease Control and Prevention (CDC) were passaged on mycoplasma negative Vero cells (ATCC #CCL-81) at the MOI of 0.005 for 48 h. Supernatant and cell lysate were combined, subjected to a single freeze–thaw, and then centrifuged at 3,000 rpm for 10 min to remove cell debris. Virus stock was poured into a 15-cm petri dish and irradiated in a Bio-Rad GS Gene Linker UV Chamber (Bio-Rad Laboratories, Inc., Hercules, CA) on the "sterilize" setting twice for 90 s with a brief swirl in between. The virus's complete inactivation was confirmed by standard plaque assay or 50% tissue culture infectious dose ($TCID_{50}$). All live virus manipulations were performed in a biosafety level 3 laboratory, and procedures were approved by the University of Arizona's Institutional Biosafety Committee. Stock concentration was 1.6×10^7 PFU/mL in DMEM, corresponding to 10 pg/μL. Typical viral loads in saliva during the first week of symptoms can range from 10^1 to 10^5 copies/μL (11). Considering 1 copy is approximately 1 fg (12), this corresponds to an expected clinical range from 10 fg/μL to 100 pg/μL. The stock SARS-CoV-2 was spiked into 10% pooled human saliva (IRHUSL250ML; Innovative Research; Novi, MI) diluted in 0.9% w/v sterile NaCl (Addipak®, Teleflex Medical, Research Triangle Park, NC), simulating the conditions of saline gargle clinical samples tested later. The final concentration of SARS-CoV-2 in the simulated samples ranged from 10 ag/μL to 10 pg/μL.

Clinical saline gargle samples

Individuals were given 5 mL of 0.9% w/v sterile NaCl (Addipak®, Teleflex Medical) and completed a 5-second swish followed by a 10-second gargle, all repeated 3 times, before sample collection. All clinical gargle samples were divided into aliquots, 1 for the smartphone antigen assays that were stored at −80°C and the other for the RT-qPCR assays performed immediately. All samples were extracted using either Direct-zol RNA Purification Kit (ZYMO Research, Irvine, CA) or QIAamp Viral RNA Minikit (Qiagen, Venlo, Netherlands), and according to the manufacturer's protocol. Extracted RNA was immediately quantified by a RT-qPCR assay on the Applied Biosystems 7300 Real-Time PCR System (Applied Biosystems, Waltham, MA) for 45 cycles. Following CDC guidelines and protocols, the SARS-CoV-2 (2019-nCoV) CDC RUO primers were used, which target the nucleocapsid (N1 and N2) gene and RNase P (RP) gene as a positive control. For this work, we analyzed 1 chip (with 4 channels) per clinical sample using the same technique used to assay simulated samples. The chip's summed immunoagglutination area (averaged over 4 channels) was placed on the clinical sample figure against its respective Ct value. No standard error was used as only 1 chip was tested per sample.

Assay procedure

Each simulated concentration was tested on 3 different paper-based microfluidic chips, each with 4 channels, thus 12 channels in total. A total of 4 μL of the clinical sample was added to the inlet of each channel. After 5 min (or until the loaded channel changed to a light gray color), 4 μL of antibody-conjugated fluorescence particles were added. Chips were covered with a box to prevent photobleaching of the loaded fluorescence particles. After 10 min (or once the loaded channels on the paper microfluidic chip were completely dry), the chip was locked into the chip holder and slid

into the device's translational stage. Using the Pro setting on the Samsung Camera app, 4 images were taken per channel, starting from the particle front (the farthest area that the particles flowed within the channel) and moving the FOV toward the loading inlet. Specifically, the first image was taken just before the particle front. Then, moving toward the loading inlet, the knob would be used to scroll beyond the field of view (FOV) of the first image, so that there would be no overlap within the images. This was repeated until 4 images were taken between the channel inlet and the particle front, a length which consistently spanned approximately 3–4 mm. While some adjustments to the microscope's focus were sometimes required during this process, the chip holder served to flatten the paper chip, eliminating much of the refocusing previously required (10), while moving along the channel. This imaging procedure would be repeated for each channel being analyzed. The use of the device can be observed in Videos S1 and S2 (Supplementary Material).

Image analysis

Images were analyzed using ImageJ (US National Institutes of Health, Bethesda, MD) with the use of a macro for particle analysis and data extraction (Figure S10, Supplementary Material). Each image was converted to 8-bit grayscale, and subsequently thresholded using a thresholding tool in ImageJ to make a binary distinction between fluorescing particle aggregates and background. After thresholding, we used the "Analyze Particles" function in ImageJ to collect a list of all fluorescing particle aggregate areas. This data was then exported into Microsoft Excel, where an additional minimum size threshold of 30 pixels was used to eliminate any remaining noise and nonaggregated singlet particles. A maximum size threshold of 10,000 was used to eliminate extremely large-size particles (e.g. hair-like fibers); however, this was not common and only occurred occasionally (e.g. only once in our clinical sample analysis). The average pixel sum over 4 channels was used to represent a single chip's data point. The standard curve shown in this paper was averaged across 3 different chips.

Analytical specificity test

Using the same technique, we loaded 3 chips with influenza A/H1N1 virus (NATFLUAH1-ERCM; ZeptoMetrix, Buffalo, NY) diluted to 1 pg/μL. The average pixel sum of immunoagglutinated particles across 3 chips (12 channels) was plotted with the standard error ($n = 3$). This result was compared to those from the standard curve for 0 and 1 pg/μL UV-inactivated SARS-CoV-2 simulated samples.

Statistical analysis

A one-tailed t-test with unequal variances was used for the statistical analysis of significance between negative and positive SARS-CoV-2 simulated samples. For the clinical sample assay, sensitivity, specificity, and accuracy were determined by setting a cutoff value to separate positive and negative results based on the average particle sum of the chips tested. Thus, positive chips with particle sums above the cutoff are determined true positive, and negative chips below the cutoff are true negative.

Biosafety and institutional review board approvals

SARS-CoV-2 virus culture was conducted and UV-inactivated in Dr Nikolich-Žugich's laboratory at Biosafety Level 3. All human clinical samples were heat-inactivated, followed by RT-qPCR in Dr Worobey's laboratory at Biosafety Level 2. All smartphone assays were conducted using the UV- or heat-inactivated samples in Dr Yoon's laboratory at Biosafety Level 2. All experimental protocols and sample collection procedures were approved by the University of Arizona's Institutional Review Board (IRB), number 2102491314.

Results and Discussion

Smartphone-based fluorescence microscope

Since the device from our previous work (10) had several limitations, it has been substantially improved in this work, as shown in Figure 2. The expanded view of the device is shown in Figure 2A. The device was modified to be foldable and more compact (Figure 2D and E), with a stand that allows any smartphone to be securely lined up with the microscope lens. We replaced thick (previously 2.5-mm thick) and expensive optical bandpass filters with inexpensive color filter films and used a newer microscope attachment. With these improvements, we acquired high-contrast and high-quality fluorescent images without noticeable aberration and for a significantly cheaper price. The device's total cost (excluding the cost of a smartphone) is less than $50 (Table S1, Supplementary Material). The images obtained from our device are comparable to the images obtained from a conventional microscope (Nikon Eclipse TS100, Minato, Tokyo, Japan), as shown in Figure S8 (Supplementary Material). Additional modifications included a translational stage system to provide smooth and precise movement along both x- and y-axes (Figure 2A and B), and use of 2 light sources, including illumination light (white light for general chip observation) and excitation light (for generating the fluorescence signal), powered by a 9 V battery (Figure 2C). Once the chip was manually inserted and the channels were located, the chip was easily moved along the length of the channels by turning a knob to slide the translational stage. This allowed for any point on the microfluidic chip to be imaged, a significant improvement to earlier designs of the smartphone-fluorescence microscope. Despite these improvements, this new version still involves some manual tedium, and therefore does not allow for exact reproducibility of the chip imaging process. However, the platform is significantly easier to use and is well-suited for automated motion control to create a user-friendly, commercial instrument. Design and optimization details can be found in Figures S1–S9 (Supplementary Material).

Paper-based microfluidic chip and assay procedure

The paper-based microfluidic chip was designed and optimized. Contrary to the previous study (10), we placed the loading area at 1 side of the channel, where we sequentially loaded the samples and reagents. This change allowed easy and reproducible identification of the microscope's FOV. It also forced the liquid to flow in 1 direction (compared to the nonreproducible bidirectional flow). In addition, a chip holder and chip lock were newly designed (Figure 2B) to flatten the paper-based chip easily, making the microscopic focusing substantially more consistent as the FOV was moved along the channel. The sample and reagent loading steps remained similar to the previous study (10), however, the new knob and translational stage significantly increased the ease of imaging along each channel. If the paper chip was visibly dirty and had many large clumps, we eliminated the entire channel without proceeding to image analysis. This occurred only once in our clinical sample analysis, and due to the limited sample volume, we could not repeat the experiment, so

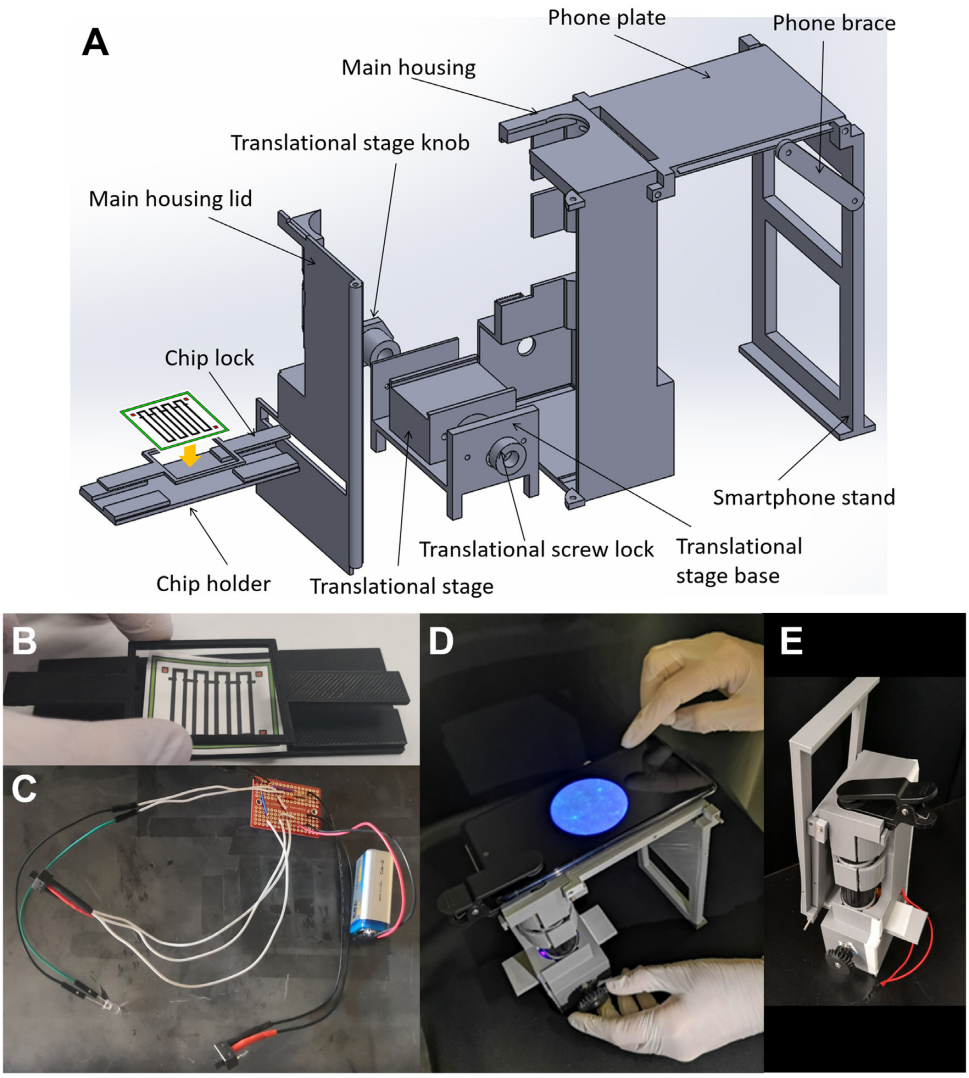

Fig. 2. Device design. (A) Expanded view of the smartphone-based fluorescence microscope, with SolidWorks diagram and parts assembly of the device. (B) A paper-based microfluidic chip is placed and flattened using a chip holder. (C) Circuit photograph for 2 light sources (blue light for fluorescence imaging and white light to more easily determine the location on the chip). The switches hang outside the device for easy access, while the battery and circuit board sit inside next to the microscope attachment. The LEDs are positioned above the paper chip, pointing downward. (D) Final device demonstration. (E) The device is foldable for portability.

we analyzed only 3 of the 4 channels in this case. We recommend that future studies enforce a protocol of simply redoing any channels with particles larger than 10,000 pixels, because in our experience, this does not represent true immunoagglutination, but is the result of self-aggregation or chip contamination. Strict adherence to particle and chip preparation will also help avoid any contamination of the chip. In this manner, the pixel areas representing only the immunoagglutinated particles will be evaluated.

LOD, assay range, and analytical sensitivity

The assay was optimized for SARS-CoV-2-spiked saliva samples. All concentrations were significantly different from NTC ($P < 0.05$) and the LOD was 10 ag/μL. Since the sample volume per channel is 4 μL, this LOD corresponds to 40 ag or 0.04 copies per channel. This low LOD is theoretically possible, as the assay detects antigen fragments rather than intact viruses with RNA (which RT-qPCR requires). It should be noted that these assays were performed on UV-inactivated samples, which may have a different concentration of fragments than those naturally occurring in intact virion solutions. The selected assay conditions were: (1) imaging 10 min after reagent loading, (2) use of polyclonal antibodies, (3) loading the sample first followed by reagent (antibody-conjugated fluorescent particles), and (4) addition of Tween 20 to the antibody-conjugated fluorescent particles (as demonstrated previously (10); Figure S11 [Supplementary Material]). Unlike the other rapid immunoassays, reagents and antibodies do not need to be immobilized on the assay platform. Using a series of solutions with 10% saliva and 0.9% saline spiked with SARS-CoV-2, standard curves were constructed, 1 for the low (10 ag/μL–1 fg/μL) and the other for the high (10 fg/μL–10 pg/μL) concentration ranges (Figure 3B). Above 1 fg/μL, the pixel area decreased, indicating saturation of antibody binding sites. The high-concentration-range standard curve showed a linear increase from 10 fg/μL to 10 pg/μL (or 40–40,000 copies per channel) for higher concentrations. To explain the overall lower signals at higher concentrations (above 1 fg/μL), we conducted additional experiments by adding Tween 20 and incubating for 30 min to the spiked saliva samples. (Note that Tween 20 was already added to the antibody–particle suspension to

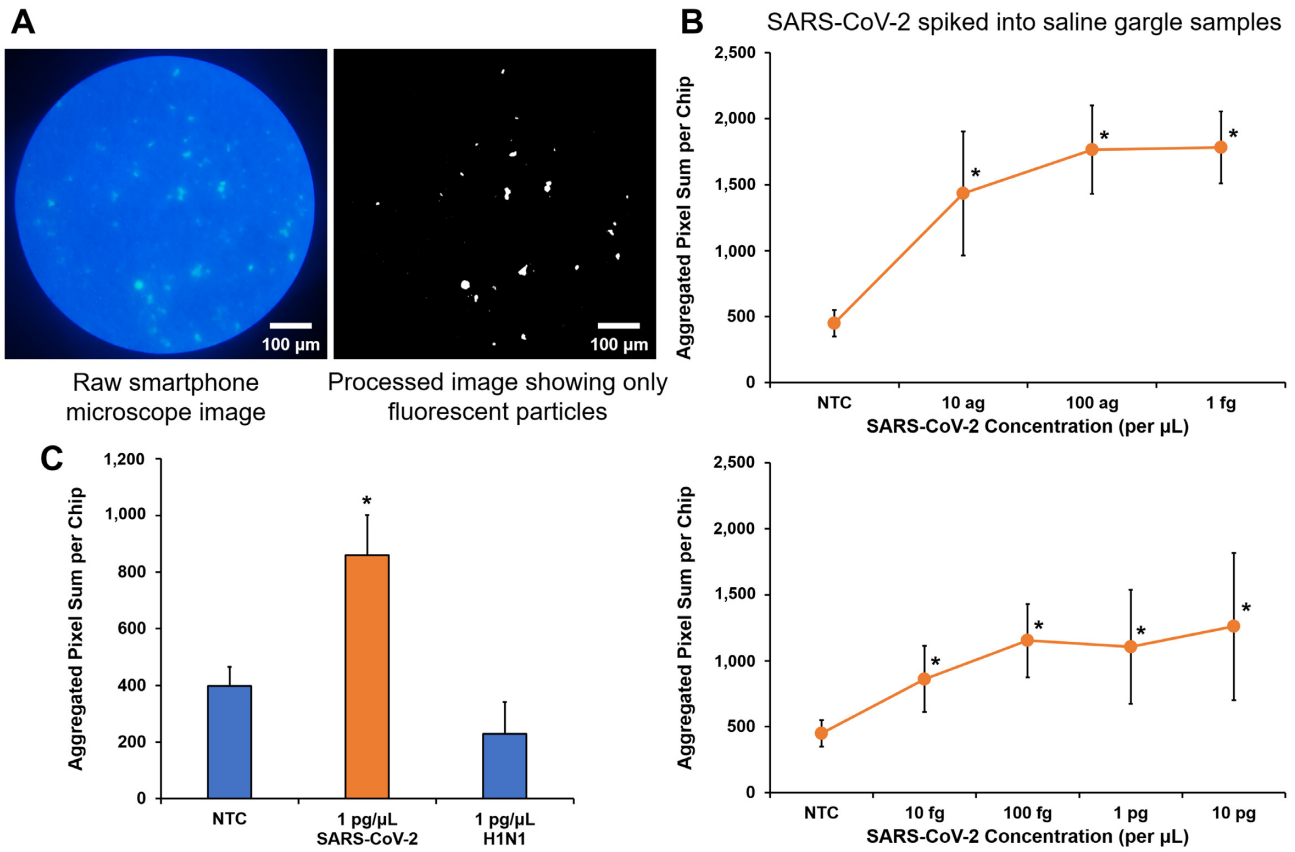

Fig. 3. Assay results: image processing, LOD, and analytical specificity. (A) After loading the sample and particles, each channel was imaged, and images were analyzed in ImageJ. The threshold was adjusted using the histogram tool until only the fluorescent particles were shown, followed by binarization. The individual areas of each white spot were collected, and any areas below 30 or above 10,000 pixels were excluded. The immunoagglutinated areas were summed in each image. (B) Standard curves were created using a series of SARS-CoV-2 spiked into saline gargle samples (10% saliva and 0.9% saline; $n = 3$ for each concentration, each time using a different chip). (C) Analytical specificity to SARS-CoV-2 was tested using negative and positive (1 pg/μL) SARS-CoV-2 samples, and influenza A/H1N1 (Ct value = 25–28), all in 10% saliva and 0.9% saline ($n = 3$ for each sample, each time using a different chip).

minimize particles' self-aggregation, although their interactions with the virus antigens should be minimal considering the short assay time and the lateral-flow characteristics.) The results are shown in Figure S12 (Supplementary Material). When a low concentration of Tween 20 was added to the SARS-CoV-2 samples, the signals of low concentrations were attenuated down to the level of NTC. However, those of high concentrations remained roughly the same (with larger error bars) as those without Tween 20 added to the SARS-CoV-2 samples. The self-aggregation of virus particles could explain this result, which would significantly attenuate the accessibility of viral antigens to the antibody-conjugated particles. Virion–virion binding is a known phenomenon for increasing the virus's ability to infect cells (13–15). Further increasing the Tween 20 concentration made the curve essentially flat across all concentrations tested. Therefore, 2 different linear ranges were identified, as shown in Figure 3B. It may be possible to pretreat the samples with Tween 20 for 30 min to distinguish high from low SARS-CoV-2 concentrations. However, such practice is impractical for clinical testing since it adds additional time and labor, and the current standard practice requires the distinction only of positive vs. negative results.

A small extent of particles' self-aggregation was noticed with the NTC samples, as shown in Figure 3B. However, they were significantly lower than all other concentrations and did not adversely affect the ability to detect the positive samples.

An additional test was performed to evaluate the analytical specificity using influenza A/H1N1 (NATFLUAH1-ERCM from ZeptoMetrix). There was no significant difference between negative simulated samples and influenza A/H1N1 (Ct value = 25–28) samples. In contrast, a significant difference was found between influenza A/H1N1 samples and positive (1 pg/μL) SARS-CoV-2 samples ($P < 0.05$; Figure 3C), successfully demonstrating the analytical specificity to SARS-CoV-2.

Clinical assays

Assays were repeated with clinical saline gargle samples. Each data point in Figure 4 represents a sample from an individual patient, assayed on 1 chip with 4 channels. All images were analyzed to acquire total pixel sums of particle immunoagglutination, which was then averaged across the channel. Clinical samples were delivered in 2 rounds, 1 in December of 2020 and the other in March 2021. The samples received in March of 2021 exhibited significantly higher turbidity and colorations, possibly due to contamination from food or oral hygiene products due to the patients' noncompliance with instructions. Due to higher turbidity and coloration, round #2 samples were sedimented using a minicentrifuge at 6,000 rpm for 10 s. Only the supernatant was loaded onto the paper-based microfluidic channel to help eliminate any food, toothpaste, or other contaminants. This

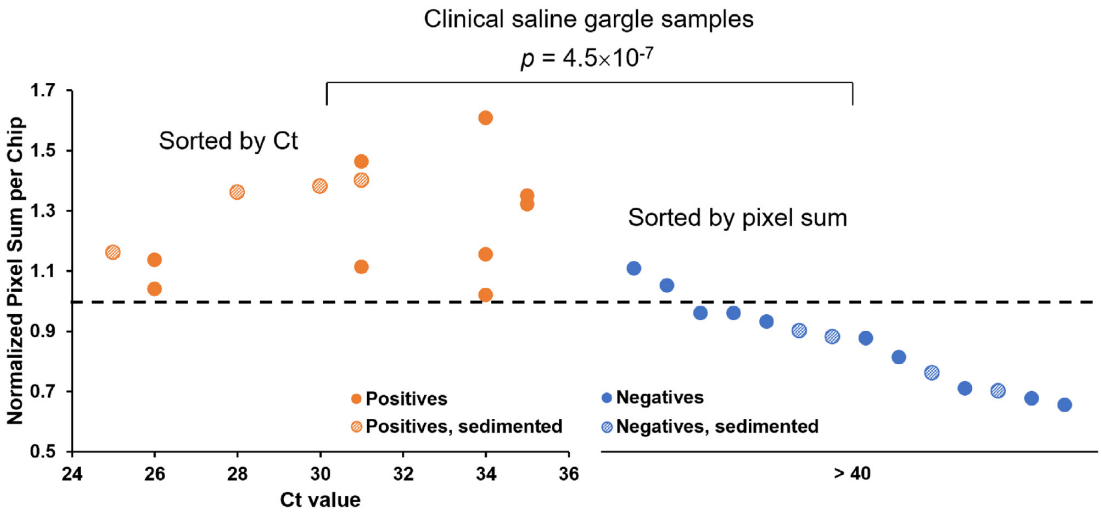

	Round #1	Round #2	Overall
Positives	9	4	13
Negatives	10	4	14
Clinical sensitivity	100%	100%	100%
Clinical specificity	80%	100%	86%
Clinical accuracy	89%	100%	93%

Fig. 4. Clinical saline gargle assay results. Solid blue and orange ($n = 19$) samples were tested in round #1 without any sedimentation, and patterned ($n = 8$) samples were tested in round #2 with sedimentation. All pixel sums were normalized by 1,700 pixels for all round #1 and 500 pixels for all round #2 samples, creating the overall cutoff line of 1. A sample of the raw images is available in Figure S13 (Supplementary Material). Clinical sensitivity, specificity, and accuracy of clinical saline gargle sample assays are shown at the bottom. Positive and negative samples showed significant difference by paired t test ($P < 0.05$).

Table 1. Performance metrics for the smartphone-based assay demonstrated in this work vs. the gold standard RT-qPCR method published in the literature for SARS-CoV-2 detection. TP = true positive, TN = true negative, FP = false positive, and FN = false negative. Note: RT-qPCR was assumed to be 100% correct for generating the performance metrics for this smartphone-based assay.

Performance metric	Definition	RT-qPCR(%) (references)	This method (%)
Clinical sensitivity	TP/(TP + FN); demonstrates ability to detect infected patients; high is desired	90–100 (16, 17)	100
Clinical specificity	TN/(TN + FP); demonstrates ability to rule out noninfected patients; high is desired	96–100 (16, 17)	86
False positive rate	FP/(FP + TN); demonstrates how frequently noninfected patients are falsely diagnosed positive; low is desired	0–4 (16, 17)	14

sedimentation may have resulted in a loss of virus and saliva samples, resulting in different pixel sum values. Hence, separate threshold decision boundaries were generated for each data set—1,700 pixels for all round #1 data and 500 pixels for all round #2 data, and data points were normalized to these values to generate a single plot. No significant batch-to-batch and channel-to-channel variations could be found within the same round of samples. As shown in Figure 4, a clear separation can be observed between positive (Ct ≤ 35) and negative samples, as confirmed by RT-qPCR (using CDC RUO primers). Clinical sensitivity (true positive/[true positive + false negative]), clinical specificity (true negative/[true negative + false positive]; this is different from the analytical specificity shown in Figure 3C), and clinical accuracy ([true positive + true negative]/all data) were summarized in Figure 4 for round #1 (nonsedimented), round #2 (sedimented), and all data. Only 2 negative samples out of 19 were identified as positive (false positive). There were no false negatives (i.e. 100% sensitivity). Table 1 summarizes the performance metrics of this smartphone-based assay compared to the gold standard RT-qPCR reported in the literature. As with the simulated samples discussed in the previous section (LOD, assay range, and analytical sensitivity), the heat inactivation step might have increased fragmentation of the target nucleocapsid protein and influenced the high clinical sensitivity achieved with this assay. Further studies on unmodified clinical samples would provide further information on the potential effects of heat inactivation.

Conclusions

We successfully developed a platform and assay for rapid detection of SARS-CoV-2 from saline gargle samples. Our complete sample-to-answer assay time for a single sample was 20 min. As stated previously, 1 of the main advantages of using saliva as a diagnostic fluid is self-collection without requiring trained personnel. While the present work focuses on detecting SARS-CoV-2 antigens, our promising assay and device could be adapted toward an antibody detection platform for SARS-CoV-2 and other viral infections. There is evidence that specific antibodies against infectious

diseases can be quantified in saliva (18). Variants of SARS-CoV-2 might be detectable using this current platform, as some research has found that many variants have not had significant changes to the nucleocapsid protein (19). Furthermore, our assay is also easily adaptable, as the particle conjugation step can be made specific to any new variant once the appropriate antibody becomes commercially available. Additionally, our wax-printed microfluidic chips could be used to provide multitarget detection of SARS-CoV-2 and its variants on a single chip. Furthermore, this platform can be adapted for antibody (instead of antigen) detection. Despite lower total concentrations of antibodies in saliva, serum and salivary IgG concentrations are present in similar proportions for a given individual (20). Such a platform would be useful for evaluating vaccine effectiveness.

Supplementary Material

Supplementary material is available at *PNAS Nexus* online.

Acknowledgments

The authors acknowledge Dr. Deepta Bhattacharya and Dr. Ryan Sprissler at the University of Arizona College of Medicine, Tucson, Arizona, United States, for the helpful suggestions and discussions on this project. The authors would also like to acknowledge the undergraduate students Jacob Baker who assisted with device development, and Hasina Shir and Samantha Mata-Robles who assisted with the experiment and materials preparation.

Funding

This project was funded by the University of Arizona's Test All Test Smart program and Tech Launch Arizona's Asset Development program. L.E.B. acknowledges partial fellowship support from the University of Arizona NASA Space Grant Graduate Fellowship. P.A. acknowledges fellowship support from the Royal Thai Government Scholarship from the Ministry of Higher Education, Science, Research, and Innovation, Thailand. K.S. acknowledges the Computational and Mathematical Modeling of Biomedical Systems Training Grant from the National Institute of General Medical Sciences (NIGMS), the US National Institutes of Health, grant number GM132008.

Authors' Contributions

J.Y.Y. conceived the overall concept with input from L.E.B., B.T.N., P.A., and K.S.; P.A. and B.T.N. designed and fabricated the smartphone-based fluorescence microscope and its 3D-printed enclosure and chip holder, with input from L.E.B. and K.S.; L.E.B. optimized the protocol of antibody conjugation to particles with input from K.K.; all preliminary data and optimization assays were performed and analyzed by L.E.B., B.T.N., P.A., and K.S.; clinical and simulated assays were performed and analyzed by L.E.B. and B.T.N.; image-processing algorithms and protocols were conceived and developed by L.E.B. and B.T.N. with input from K.S. and P.A.; spiked samples were prepared by B.T.N. using SARS-CoV-2 cultured by J.U. and J.N.Z.; clinical samples were collected and tested by G.Q. and M.W.; L.E.B., B.T.N., P.A., K.S., and J.Y.Y. wrote the manuscript and Supplementary Materials; and J.N.Z., M.W., and J.Y.Y. secured the funding, supervised the personnel, and oversaw the collaborative project. All authors have approved the final version of the manuscript.

Data availability

Protocol for covalent coupling of antibodies to the fluorescent particles is available at protocols.io at https://doi.org/10.17504/protocols.io.bhsvj6e6. Protocol for wax printing the paper-based microfluidic chips is available at protocols.io at https://doi.org/10.17504/protocols.io.btqxnmxn. All data associated with this study are present in the paper and the Supplementary Materials.

References

1. CDC (U.S. Centers for Disease Control and Prevention). 2021. Interim guidelines for collecting and handling of clinical specimens for COVID-19 testing (CDC, 2021). https://www.cdc.gov/coronavirus/2019-ncov/lab/guidelines-clinical-specimens.html. [accessed 2021 May 17].
2. Sheridan C. 2020. Fast, portable tests come online to curb coronavirus pandemic. Nat Biotechnol. 38:515–518.
3. Cheng C, Cui H, Wu J, Eda S. 2017. A PCR-free point-of-care capacitive immunoassay for influenza A virus. Microchim Acta. 184:1649–1657.
4. Abbott. 2020. COVID-19 testing basics. https://binaxnow.workplace.abbott/covid-testing. [accessed 2021 May 31].
5. Smithgall MC, Dowlatshahi M, Spitalnik SL, Hod EA, Rai AJ. 2020. Types of assays for SARS-CoV-2 testing: a review. Lab Med. 51:e59–e65.
6. Corstjens PLAM, Abrams WR, Malamud D. 2012. Detecting viruses by using salivary diagnostics. J Am Dent Assoc. 143:12S–18S.
7. Worobey M. 2020. Swish, gargle, repeat: UArizona researcher explores mouth rinse test as Alternative to COVID-19 nasal Swab. UANews. https://news.arizona.edu/story/swish-gargle-repeat-uarizona-researcher-explores-mouth-rinse-test-alternative-covid-19-nasal. [accessed 2021 Jun 20].
8. Perchetti G, Huang M-L, Mills MG, Jerome KR, Greninger AL. 2021. Analytical sensitivity of the Abbott BinaxNOW COVID-19 Ag Card. J Clin Microbiol. 59:e02880–e02820.
9. Prince-Guerra JL, *et al.* 2021. Evaluation of Abbott BinaxNOW rapid antigen test for SARS-CoV-2 infection at two community-based testing sites — Pima County, Arizona, November 3–17, 2020. MMWR Morb Mortal Wkly Rep. 70:100–105.
10. Chung S, *et al.* 2021. Norovirus detection in water samples at the level of single virus copies per microliter using a smartphone-based fluorescence microscope. Nat Protoc. 16:1452–1475.
11. Zhu J, Guo J, Xu Y, Chen X. 2020. Viral dynamics of SARS-CoV-2 in saliva from infected patients. J Infect. 81:e48–e50.
12. Bar-On YM, Flamholz A, Phillips R, Milo R. 2020. SARS-CoV-2 (COVID-19) by the numbers. eLife. 9:e57309.
13. Cuevas JM, Durán-Moreno M, Sanjuán R. 2017. Multi-virion infectious units arise from free viral particles in an enveloped virus. Nat Microbiol. 2:17078.
14. Andreu-Moreno I, Sanjuán R. 2018. Collective infection of cells by viral aggregates promotes early viral proliferation and reveals a cellular-level Allele effect. Curr Biol. 28:3212–3219.
15. Sanjuán R, Thouluze M-I. 2019. Why viruses sometimes disperse in groups. Virus Evol. 5:vez014.
16. Kubina R, Dziedzic A. 2020. Molecular and serological tests for COVID-19. A comparative review of SARS-CoV-2 coronavirus laboratory and point-of-care diagnostics. Diagnostics. 10:434.

17. Pu R, *et al.* 2022. The screening value of RT-LAMP and RT-PCR in the diagnosis of COVID-19: systematic review and meta-analysis. J Virol Meth. 300:114392.
18. Parry JV, Perry KR, Mortimer PP. 1987. Sensitive assays for viral antibodies in saliva: an alternative to tests on serum. Lancet. 330:72–75.
19. Ye Q, Lu S, Corbett KD 2021. Structural basis for SARS-CoV-2 nucleocapsid protein recognition by single-domain antibodies. Front Immunol. 12:719037.
20. Hettegger P, *et al.* 2019. High similarity of IgG antibody profiles in blood and saliva opens opportunities for saliva based serology. PLOS ONE. 14:e0218456.